

ARTICLE

Open Access

Phase-multiplied interferometry via cavity dynamics for resolution-enhanced coherent ranging

Yifan Wang¹, Jinsong Liu¹, Chenxiao Lin¹, Xin Xu¹, Yu Wang¹, Xinhang Yang¹, Binbin Xie¹, Jibo Han², Tengfei Wu², Xuling Lin³, Liangcai Cao¹, Hongbo Sun¹ and Yidong Tan¹✉

Abstract

Coherent light detection and ranging (LiDAR) has become an indispensable tool in autonomous systems, offering exceptional precision and ambient-light immunity. Recently, applications spanning from scientific research to advanced manufacturing have increasingly required resolution that exceeds current capabilities, which faces a fundamental trade-off between improved performance and system complexity. In this study, we overcome the intrinsic limitation and present a cavity dynamics-enabled approach that actively enhances the ranging resolution through phase multiplication. By injecting target-scattered light into the optical resonator, the operating frequency of the laser undergoes periodic modulation, generating interference harmonics that multiply the phase sensitivity. Experimentally, we observe the excitation of up to the 13th-order harmonic and effective phase multiplication without physical modulation extensions, which enables more than 10 times resolution enhancement for ranging. Owing to the intrinsic phase correlation between the fundamental wave and harmonic waves, the phase noise is effectively controlled, resulting in high-precision ranging with a standard deviation on the order of tens of micrometers. The system concurrently leverages laser feedback sensitivity, achieving significant signal-to-noise ratio (SNR) improvement. With its enhanced resolution, low photon consumption, and low-cost implementation, this technology demonstrates new capabilities that promise to enable a wide range of applications.

Introduction

Coherent metrology, which is known for its high precision, immunity to ambient light, and traceability, represents an important class of methods with extensive applications in both scientific and industrial fields, such as space exploration, medical diagnosis, and advanced manufacturing^{1–4}. In particular, the flourishing developments of automatic driving, precision fabrication, and 3-dimensional (3D) profilometry have driven the need for accurate and dynamic measurements^{5–9}, which are consistent with the advantages of coherent ranging methods.

Consequently, coherent ranging methods have become a focus of research, and recent advancements have significantly improved their capabilities. Chip-scale integration and parallel measurement methods increase the measurement efficiency^{10–12}, high repetition-rate modulation enables local vibration monitoring¹³, and narrow-linewidth lasers increase the measurement range¹⁴. These innovations have expanded the applicability of coherent ranging techniques in various scenarios.

Resolution is an important metric for assessing coherent ranging systems; however, most coherent ranging methods have an intrinsic trade-off between resolution enhancement and system complexity. In frequency-modulated continuous-wave (FMCW) systems, among the most prevalent coherent ranging techniques, resolution is essentially governed by the sweep bandwidth. Employing sources with extended

Correspondence: Yidong Tan (Tanyd@tsinghua.edu.cn)

¹State Key Laboratory of Precision Measurement Technology and Instruments, Department of Precision Instruments, Tsinghua University, Beijing, China

²National Key Laboratory of Metrology and Calibration, Beijing Changcheng Institute of Metrology & Measurement, Beijing, China

Full list of author information is available at the end of the article

These authors contributed equally: Yifan Wang, Jinsong Liu, Chenxiao Lin

© The Author(s) 2026



Open Access This article is licensed under a Creative Commons Attribution 4.0 International License, which permits use, sharing, adaptation, distribution and reproduction in any medium or format, as long as you give appropriate credit to the original author(s) and the source, provide a link to the Creative Commons licence, and indicate if changes were made. The images or other third party material in this article are included in the article's Creative Commons licence, unless indicated otherwise in a credit line to the material. If material is not included in the article's Creative Commons licence and your intended use is not permitted by statutory regulation or exceeds the permitted use, you will need to obtain permission directly from the copyright holder. To view a copy of this licence, visit <http://creativecommons.org/licenses/by/4.0/>.



sweep ranges offers a direct pathway to resolution improvement. Conventional solutions such as external cavity diode lasers (ECDLs) have limitations because of mechanically constrained tuning speeds despite their terahertz-scale bandwidths^{8,15}. Alternative swept sources, including vertical cavity surface emitting lasers with micro-electromechanical systems-based tuning mechanisms (MEMS-VCSELs)^{16–18}, Fourier domain mode-locked lasers (FDMLs)^{19,20}, time-stretching lasers^{14,21,22}, and stitched-DFB arrays^{23,24}, offer exceptional bandwidth performance. Their bandwidths reach tens of nanometers or greater, enabling micrometer-scale resolution at modulation frequencies near 100 kHz. Nevertheless, these approaches exhibit significant complexity in source control and signal analysis. Furthermore, multiwavelength interferometry requires multiple precisely wavelength-stabilized sources, because resolution critically relies on wavelength combinations^{25,26}. Frequency-comb-based coherent ranging methods achieve high resolution. However, as reported for dual-comb-based^{27–33}, repetition-rate-modulated⁶, and carrier-envelope-offset frequency-modulated¹¹ approaches, stringent frequency locking in addition to extra optical amplifiers and costly instrumentation is necessary. Consequently, implementing high-resolution ranging using a simple system remains challenging.

With respect to signal analysis, the phase of the interference signal in coherent ranging allows for measurement result demodulation, and the sensitivity to phase increments determines the achievable resolution of systems^{24,34}. Thus, phase manipulation, through multiplication, noise reduction, or correlation analysis, offers a pathway to resolution enhancement without solely relying on hardware extensions. Techniques such as beat signal mixing^{35,36} and deep learning-based signal prediction³⁷ are promising in this regard. However, these methods have limited multiplication factors and extensive prior data requirements, which hinder real-time, high-precision applications.

In this study, we present a laser-feedback-based phase multiplication (LFPM) method for resolution-enhanced coherent ranging, which exploits nonlinear effects in cavity dynamics to multiply the interference signal phase. Laser feedback occurs when the output light partially returns to the resonator^{38–40}. The reinjected light interferes with the intracavity light field, generating a spontaneously amplified beat signal^{41,42}, which has been reported in our previous work⁴³, and affects the cavity mode. With nonlinear cavity dynamics, the system generates harmonics of the interference signal and multiplies the phase sensitivity. Owing to the stable phase correlation between the harmonics and the fundamental wave, the phase noise in higher-order signals remains controllable, achieving tens of micrometer-level standard

deviations in practically repeated measurements. Furthermore, the system inherits the high sensitivity of laser feedback, which simultaneously provides intensity amplification across various harmonic orders to facilitate effective detection. Notably, the ability to selectively employ different harmonic orders allows for dynamic trade-offs between resolution enhancement and detection sensitivity. This intrinsic flexibility renders the LFPM technique adaptable to a broad spectrum of applications, including fiber-optic sensing, target tracking, and high-precision positioning.

In addition to laser ranging, the proposed LFPM method has the potential to enhance phase sensitivity in other coherent measurement tasks, where measurements often translate to detecting phase changes in specific physical processes^{44–46}. Compared with existing techniques, e.g., using multiphoton number and path-entangled (NOON) states, nonlinear optical crystals, and optical path multiplication^{47,48}, our method has the distinct advantages of a low excitation threshold, high harmonic multiplicity, simple structure, and low implementation complexity, rendering it applicable to various heterodyne interferometry challenges.

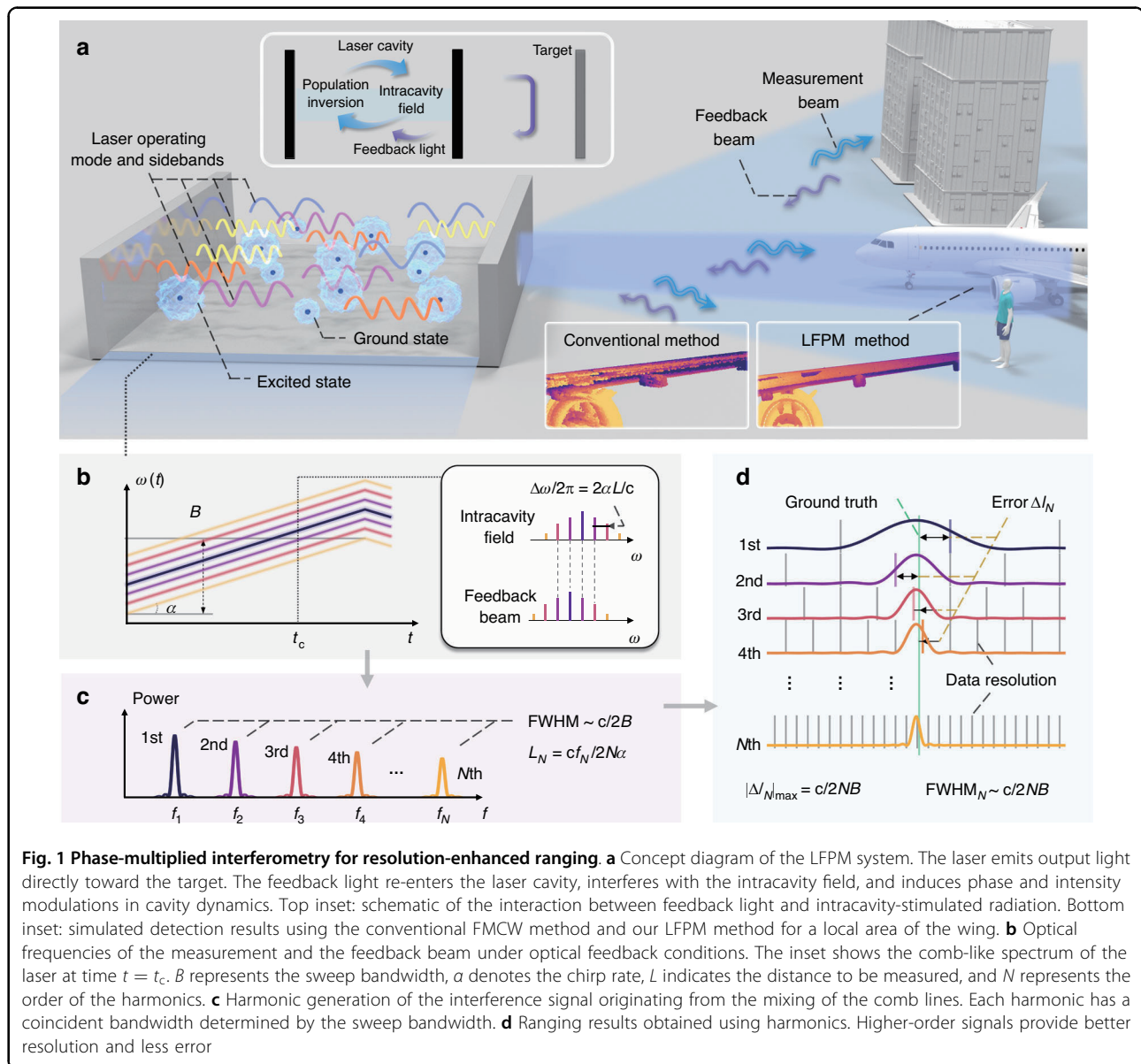
Results

Concept of the LFPM ranging system

A conceptual diagram of the LFPM ranging system is shown in Fig. 1a. A tunable laser with internal modulation emits a frequency-swept beam. The measurement beam is directed toward the target, and the backscattered light is reinjected into the laser resonator. This feedback light, delayed by time τ relative to the intracavity field, generates a beat signal through coherent mixing with the local oscillator. If the optical frequency is swept linearly with time in a single trip (with the fixed chirp rate α), the beat frequency is constant. Additionally, the feedback light participates in the stimulated emission process, periodically modulating the gain-loss parameters of the resonator at the beat frequency, resulting in dynamic modulation of the phase and intensity of the intracavity optical field.

Phase modulation manifests as the generation of new optical frequency components. Under optical feedback conditions, the laser exhibits a comb-like spectrum, as shown in Fig. 1b, where the frequency interval between the comb lines coincides with the difference between the intracavity optical field and the feedback beam. The interference between various sidebands produces the harmonics of the fundamental beat signal in Fig. 1c. Moreover, intensity modulation induced by the feedback light results in periodic fluctuations in the population inversion and gain coefficient, spontaneously amplifying the amplitude of the beat signal. Notably, when the beat frequency approaches the relaxation oscillation (RO) frequency, the typical amplification factor exceeds 10^4 .





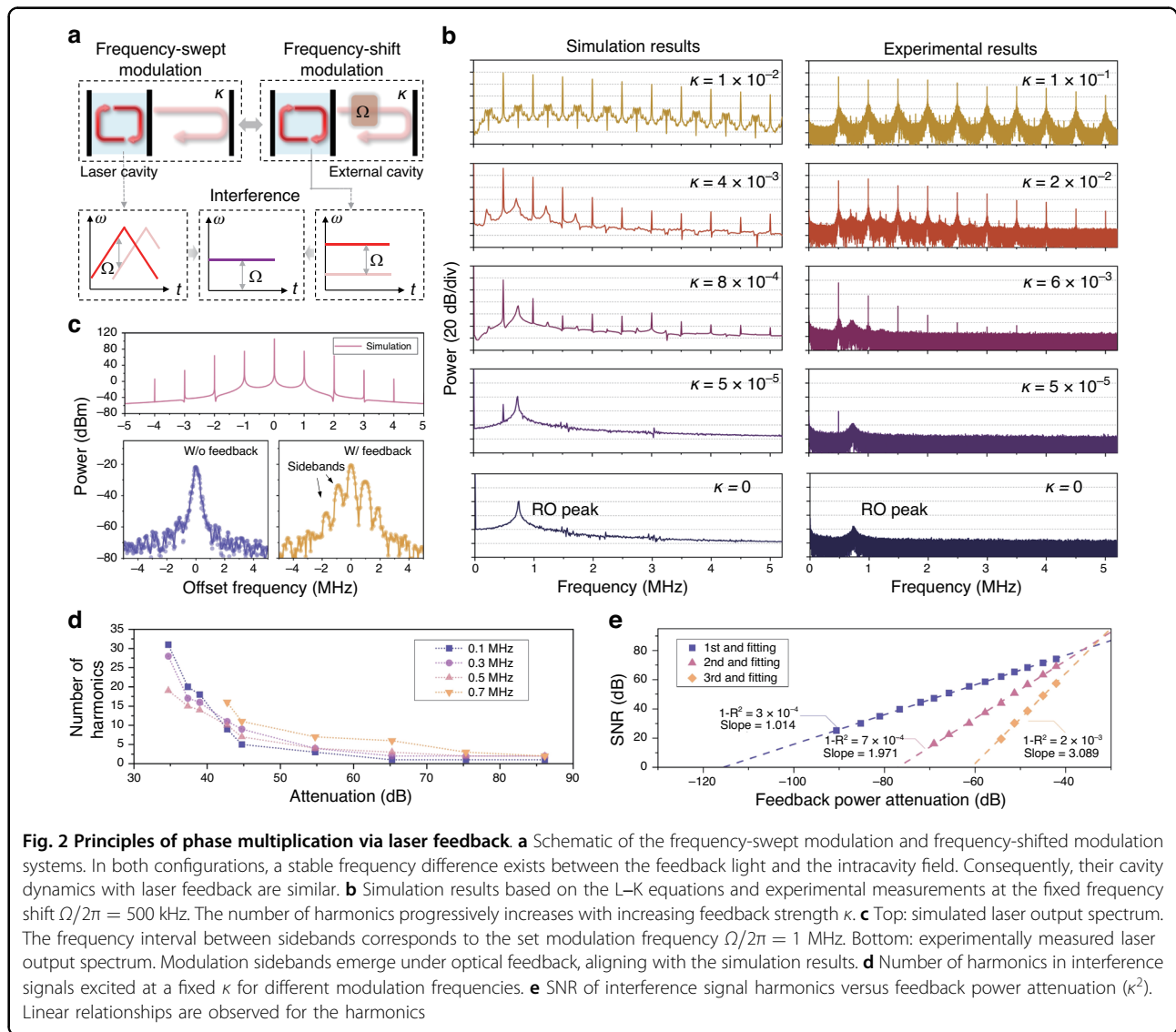
With gain saturation, the beat signal and its harmonics undergo nonlinear amplification. Overall, this laser feedback system induces nonlinear cavity dynamics and thus exhibits harmonic beat-signal generation.

The representative harmonic spectrum in the LFPM method is shown in Fig. 1c, and the full width at half maximum (FWHM) of the harmonic frequencies exhibits consistent values inversely proportional to sweep bandwidth B . This phenomenon enables a significant improvement in the ranging resolution when the N th harmonic signal is used. Because the effective sweep bandwidth is expanded by a factor of N , the beat frequency of the N th harmonic is correspondingly N times greater than that of the fundamental signal. Consequently, the raw distance obtained from the N th

harmonic must be divided by N to yield the actual target distance. Moreover, the FWHM is reduced to $1/N$ of its fundamental value. This narrower spectral linewidth indicates a finer effective frequency sampling interval. As a result, the detrimental fence-posting effect intrinsic in the discrete Fourier transform is mitigated, reducing uncertainty in locating the true peak frequency. Ultimately, this decreased peak frequency estimation error translates directly to a lower ranging error relative to the ground truth, increasing both the resolution and precision (Fig. 1d).

Principle of phase multiplication

Higher-order harmonic generation originates from the nonlinear cavity dynamics induced by laser feedback and



can be described within the semiclassical framework using rate equations. In conventional Lang–Kobayashi (L–K) feedback models^{49,50}, the phase difference between intracavity light and feedback light is the focus. To elucidate the underlying mechanism, we analyze the feedback process in a free-running source under frequency-shifted modulation to investigate that of a frequency-swept laser source, where the frequency shift corresponds to the beat frequency generated in the ranging signal, as shown in Fig. 2a. This approximation remains valid given that the cavity mode sweeping rate is substantially lower than the laser buildup rate. $N(t)$, $E_c(t)$, and $\Phi(t)$ denote the population inversion, the complex amplitude of the electric field in reduced units (photon units), and the optical phase, respectively. The rate equations with laser optical feedback are expressed

as follows:

$$\frac{dN(t)}{dt} = \gamma_1[N_0 - N(t)] - B_E N(t)|E_c(t)|^2 \tag{1}$$

$$\frac{dE_c(t)e^{i\Phi(t)}}{dt} = \left[i\omega_c + \frac{B_E N(t) - \gamma_c}{2} \right] E_c(t)e^{i\Phi(t)} + \kappa \gamma_c E_c(t - \tau)e^{i\Phi(t-\tau)}e^{i\Omega t} \tag{2}$$

where γ_1 represents the decay rate of the population inversion; $\gamma_1 N_0$ represents the pumping rate; B_E denotes the Einstein coefficient; ω_c indicates the laser cavity frequency; γ_c represents the decay rate of the photon inside the cavity; κ denotes the feedback strength, which is defined as the square root of the feedback-to-output power ratio; τ indicates the transit time of the photon in

the external cavity; and Ω represents the round-trip frequency shift of the light provided by the frequency shifter. For simplicity, we assume that the round-trip time outside the cavity is shorter than the period of the frequency-shifted modulation ($\Omega\tau \ll 1$), and $E_c(t - \tau) \approx E_c(t)$. The evolution of $E_c(t)$ can be simplified as follows:

$$\frac{dE_c(t)}{dt} = \frac{B_E N(t) - \gamma_c}{2} E_c(t) + \kappa \gamma_c E_c(t) \cos[\Omega t - \omega(t)\tau] \quad (3)$$

$$\omega(t) = \omega_c + \kappa \gamma_c \sin[\Omega t - \omega(t)\tau] \quad (4)$$

Consequently, the running laser frequency $\omega(t)$ is modulated and fluctuates regularly: the magnitude correlates with the feedback strength κ , and the period matches the modulation frequency Ω . Equation (4) reveals that the laser generates multiple modulation sidebands. Interference occurs between these sidebands, thereby generating harmonic beat signals, with frequencies $\Omega, 2\Omega, 3\Omega, \dots$, and corresponding multiple phase shifts.

On the other hand, the harmonic signal can be amplified spontaneously by cavity dynamics. Through linear perturbation analysis of Eqs. (1) and (3), the relative variation in the population inversion $\Delta n(t)$ can be derived as follows:

$$\Delta n(t) \propto \frac{\kappa \gamma_c \gamma_1 (\eta - 1)}{\sqrt{[\gamma_c \gamma_1 (\eta - 1) - \Omega^2]^2 + (\gamma_1 \eta \Omega)^2}} \cos(\Omega t - \omega_c \tau) \quad (5)$$

where $\eta = B_E N_0 / \gamma_c$ represents the normalized pumping rate. The fluctuations of population inversion, as well as the gain saturation effect, periodically modulate the optical gain and thus affect the intensity of the harmonics. Δi_N represents the relative intensity modulation of the N th harmonic, and G_N represents the gain factor.

$$\Delta i_N \propto \kappa^N G_N(N\Omega) \cos(N\Omega t - N\omega_c \tau) \quad (6)$$

Numerical simulations are performed, and the modulation frequency is 500 kHz. The numerical solution of Eq. (4) is obtained and then substituted into Eq. (3). The evolution of the normalized power spectrum of the laser output with various κ values is shown in Fig. 2b. With respect to $\kappa = 0$ (free-running), a single RO peak is observed at 750 kHz. As the feedback strength κ increases, a beat frequency signal emerges, after which harmonic signals appear. When κ exceeds 10^{-3} , the number of harmonics progressively increases, up to the 10th.

Experimental validation is conducted. An acousto-optic modulator is employed to induce a frequency shift for the feedback light. We use an adjustable attenuator to control the feedback power. The evolution of the output spectrum at various values of κ is in agreement with the simulations. Minor discrepancies in absolute feedback strength values may arise from mode mismatches (e.g., polarization or transverse modes) between the feedback light and the intracavity field. The fine laser spectra from the simulations and experiments are shown in Fig. 2c, revealing a comb-like structure with a comb-line spacing equal to the modulation frequency. The setup is shown in Supplementary Information 1. We also record the number of harmonics at other modulation frequencies. The harmonic counts corresponding to $\Omega/2\pi$ values of 100 kHz, 300 kHz, 500 kHz, and 700 kHz tend to decrease with increasing attenuation, as shown in Fig. 2d.

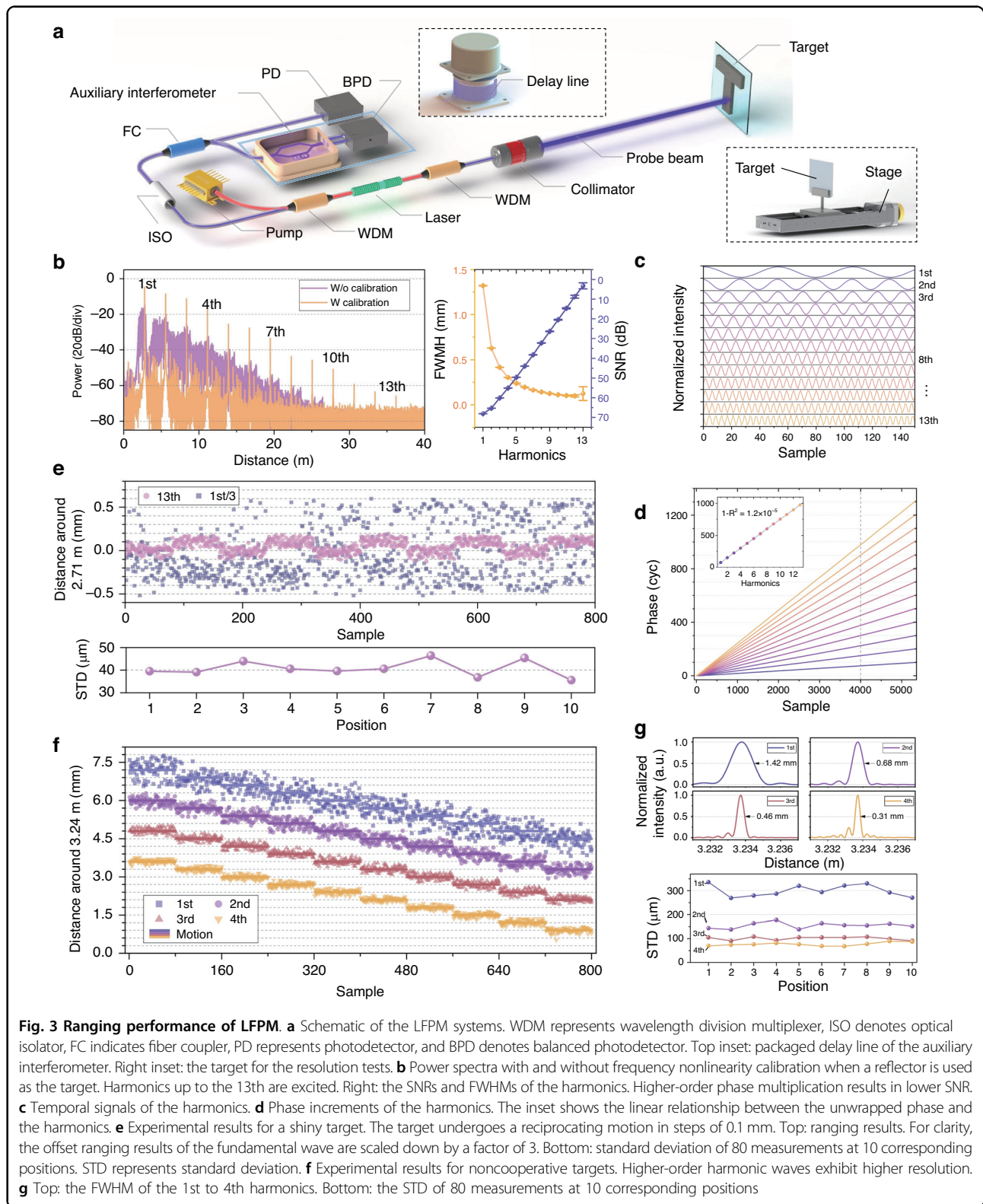
To further investigate the relationship between the feedback strength and the harmonic intensity response, we attenuate the return light to measure the signal-to-noise ratio (SNR). The attenuation curves for the 1st, 2nd, and 3rd harmonics exhibit linear responses on a logarithmic scale, as presented in Fig. 2e, and the corresponding slopes of the linear fits are 1.01, 1.97, and 3.09, respectively. This observation reveals that the intensity of the N th harmonic scales with the N th power of the feedback level. Higher-order harmonics are more sensitive to attenuation of the feedback light, which is consistent with Eq. (6). These experimental results are consistent with the simulation results, confirming the validity of our theoretical model. Notably, PD noise also affects the SNR and the number of detectable harmonics. Further details are available in Supplementary Information 2.

Ranging results with enhanced resolution

We perform absolute distance measurement experiments on the basis of our system and evaluate the performance of phase multiplication. The experimental setup is shown in Fig. 3a. The output power of the laser source is nearly 2 mW, with a maximum sweep bandwidth of 110 GHz. The main power serves as the measurement beam for ranging, whereas the minor power from the other port is split further for detection and calibration. We set up an auxiliary interferometer to calibrate the swept-frequency nonlinearity⁵¹, which is critical for high-precision distance measurement (explained in the Materials and Methods section), and the entire packaged device is monitored by a temperature controller. A photodetector (PD) is used to receive the beam from the laser. Because the beat signal is generated within the resonant cavity, directly analyzing the output light of the laser can yield the measured distance.

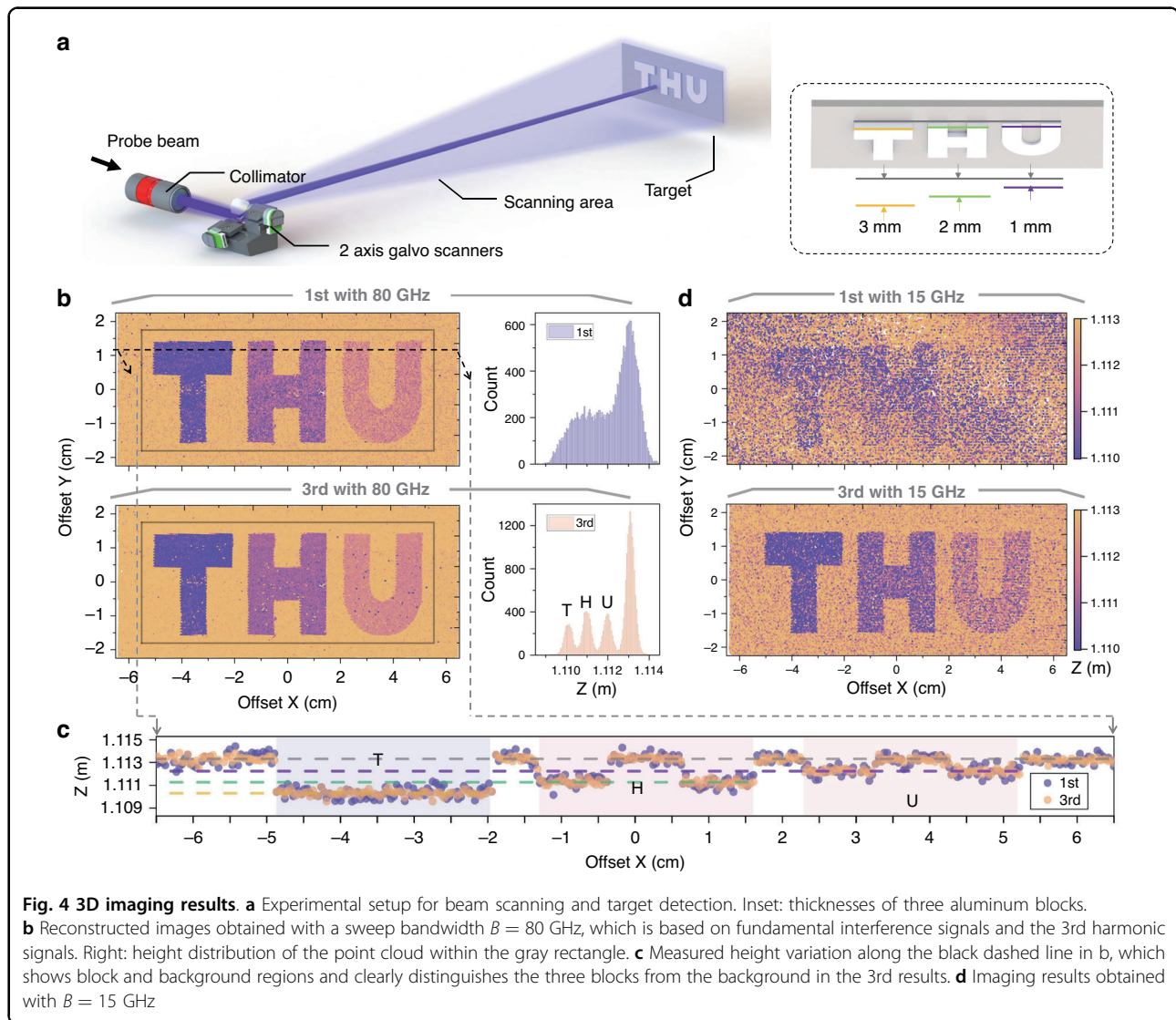
The ranging results when a reflector is employed as the target are presented in Fig. 3b. With the auxiliary





interferometer, nonlinear phase noise is suppressed, and harmonics up to the 13th order in the calibrated output spectrum are clearly observed. In contrast, prior to this

correction, adjacent harmonics are indistinguishable because of severe spectral broadening. Both the SNR and the FWHM values of the calibrated harmonics decrease



with increasing harmonic order. We separate the original interference signals during a chirp process with bandpass filters and obtain the harmonic components in the time domain. The normalized temporal signals are shown in Fig. 3c, and the Hilbert transform of these signals reveals their phase evolution in Fig. 3d. The inset, which highlights the phase increments of different harmonics at an identical time point, shows a distinct linear relationship. These observations are in agreement with our theoretical analysis and validate the capability of phase multiplication of our proposed method.

Resolution tests of the LFPM are conducted. A shiny target is displaced by 0.1 mm using a translation stage, with 80 ranging measurements obtained at each position. The fundamental frequency corresponds to a target distance of 2.71 m. As shown in Fig. 3e, the results of the 13th harmonic clearly reconstruct the motion, and the

standard deviation at each position is less than $50 \mu\text{m}$, while the results of the fundamental wave cannot be resolved. For noncooperative targets, results employing harmonics are obtained from an aluminum block at 3.24 m with an effective reflectivity of 2×10^{-6} , which is far from the mirror reflectivity. A weak feedback strength results in a decrease in the number of excited harmonics, as shown in Fig. 2e, and up to the 4th harmonic is observed in the experiments. The displacement is 0.3 mm in each step. As shown in Fig. 3f, higher harmonics progressively reconstruct the motion trajectory. The intensity-normalized interpolated spectra of the 1st to 4th harmonics, as shown in Fig. 3g, reveal a distinct decrease in the FWHM from 1.4 mm to 0.3 mm. The precision analysis, evaluated through 80 repeated measurements, reveals a standard deviation of $76 \mu\text{m}$ for the 4th harmonic, corresponding to a fourfold improvement in

measurement precision compared with the fundamental wave with 300 μm .

LiDAR and 3D imaging

The LFPM method simultaneously achieves substantial resolution enhancement and reduces the implementation complexity, revealing its potential for 3D imaging. We experimentally validate this concept using a two-axis scanning galvanometer to steer the light beam across horizontal and vertical coordinates (Fig. 4a). Three aluminum blocks (with thicknesses of 3, 2, and 1 mm along the axis) forming the letters “THU” are positioned 1.1 m from the collimator as targets. A schematic of the data acquisition is provided in Supplementary Information 3. We propose an adaptive intensity compensation method using a semiconductor optical amplifier (SOA) to compensate for the feedback power fluctuations, and the system and performance are elucidated in Supplementary Information 4.

The results obtained with an effective sweep bandwidth of 80 GHz are presented in Fig. 4b. Fourier analysis is directly applied to the calibrated beat signals without frequency-domain interpolation. After the resolution enhancement of the LFPM, the 3rd harmonic reconstructions exhibit superior fidelity compared with those of the fundamental signal. As indicated by the dashed horizontal slice in Fig. 4c, the 3rd harmonic profile shows smoother outlines with reduced noise, closely aligning with the ground truth. The deviation of each individual target is less than 200 μm , which originates from optical path fluctuations induced by the shaking of the galvanometers. Data distribution statistics are also performed to quantify the degree of concentration of the results, as shown in the histograms in Fig. 4b. The separability of the background and the three targets is significantly improved through the proposed LFPM method. The sweep bandwidth is further reduced to 15 GHz, a range achievable with conventional phase modulators. Under this condition, the measurements based on both the conventional method and the proposed LFPM method are shown in Fig. 4d. The reconstruction with the fundamental wave is difficult to resolve, whereas that with the 3rd harmonic can be clearly recognized.

Discussion

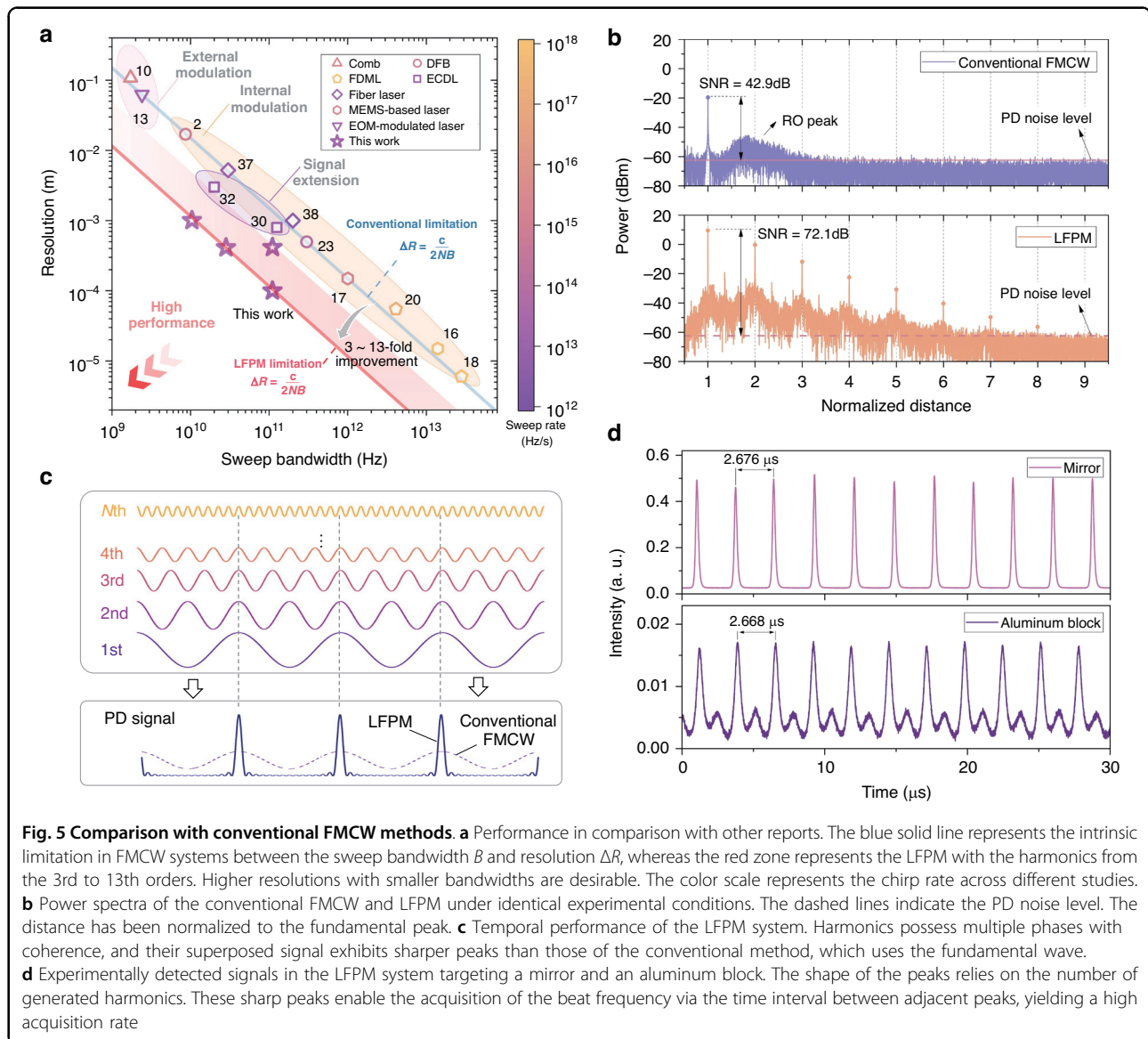
Our work establishes a technique for resolution-enhanced laser ranging. By leveraging the laser feedback effect, backscattered light interferes with the intracavity field. This process actively generates the harmonics of the beat signal through nonlinear cavity dynamics, including cavity-mode frequency modulation and gain saturation. Note that the harmonics are not spurious artifacts. Instead, they intrinsically carry phase information that is multiplicatively enhanced to increase the ranging

resolution and precision. Consequently, the laser cavity itself functions not only as a signal generator but also as an active nonlinear phase-processing element. This functionality is achieved without the need for complex external optical modulators or operating at high energy thresholds. In the experiments, the μW -level feedback power generates harmonics exceeding the 10th order, and we achieve 3-fold to 13-fold phase multiplication. In 3D imaging, our method resolves objects spaced 1 mm apart using only a 15 GHz sweep bandwidth without interpolation. Additionally, the LFPM method has a ranging capacity that is greater than 100 m, with a standard deviation on the order of tens of micrometers (Supplementary Information 5).

We compare the performance of our proposed LFPM method with that of the representative reported FMCW ranging methods in Fig. 5a. The proposed LFPM method overcomes the intrinsic limitation in frequency-domain interferometry between the resolution and sweep bandwidth and improves it toward a more desirable level. With the generation of higher-order harmonics, the performance can be improved further. With respect to phase, this harmonic-induced multiplication is equivalent to extending the effective sweep range of the system, which prevents the resolution from being limited by the physical bandwidth. This mechanism leverages the intrinsic nonlinear dynamics of the laser cavity rather than circumventing basic Fourier analysis. Compared with parallel coherent ranging systems, such as dual-comb ranging and multiwavelength interferometry, the LFPM method has a compact size and low photon consumption. Compared with NOON-state-based phase multiplication techniques, our system demonstrates a higher enhancement factor and is robust under ambient noise and vibrational interference. Furthermore, intracavity interference eliminates the need for external reference paths in our LFPM system, enabling a compact design with reduced complexity. This optimized approach has vast potential for scientific and industrial applications, including remote target tracking and positioning.

To clearly validate the generation of harmonics originating from laser cavity dynamics instead of electrical factors, we perform a comparison with a conventional FMCW-based ranging system (Supplementary Information 6). The conventional system exhibits no generation of harmonics, as shown in Fig. 5b. Moreover, the intensity response of the fundamental signal also decreases, whereas the SNR of the LFPM is nearly 30 dB greater. This distinction arises from the noise mechanisms. In conventional FMCW systems, all noise sources, particularly PD noise and laser intensity noise, decrease the SNR. Conversely, the LFPM leverages intracavity interference to render the SNR partially independent of PD noise. Optical feedback thus acts as an effective PD-noise





suppressor, significantly improving signal detectability. This improvement indicates that the proposed system is advantageous in both phase and intensity sensitivity. Notably, laser feedback achieves phase multiplication not limited to the ranging system, and it enables enhanced resolution with weak return power in other interferometric systems, such as heterodyne interferometry for displacement measurements.

Despite the advantages mentioned above, some aspects can still be improved in the LFPM system in the future. First, the laser-feedback-induced intensity amplification for the harmonics is not flat, and the response frequency bandwidth is limited by the laser dynamics (Supplementary Information 7). The gain of the amplification is associated with the frequency of the beat signal, and the maximum is achieved when the beat frequency equals the

RO frequency. The SNR and sensitivity of higher-order harmonics can be further increased through appropriate control of the self-mixing gain by matching the frequency, such as adjusting the RO frequency or adding frequency-shifted devices. Moreover, the feasible dynamic range for the feedback strength is relatively small, especially for high-order harmonics, because of the power relationship of intensity degradation. On the other hand, the feedback strength cannot increase indefinitely, and single-mode operating conditions should be guaranteed. Strong optical feedback results in multiple emission frequencies, bifurcation, mode hopping, or even chaos⁵². Consequently, there is a trade-off between the resolution enhancement and detection sensitivity, and the fundamental wave has the highest detection sensitivity. The LFPM system allows for the selection of an appropriate harmonic order to

match scenarios with different resolution and sensitivity requirements, supporting greater applicability across diverse measurement tasks.

In terms of other factors affecting performance, although this work emphasizes a novel mechanism for resolution enhancement, the effective sweep bandwidth of the LFPM, while in the THz range, remains lower than that of typical FDML or VCSEL-based FMCW systems. In our system, the available effective bandwidth relies on the maximum variation in the laser cavity length, which is achieved by mechanically stretching the whole fiber laser. To achieve higher resolution rather than merely enhancing it by phase multiplying, the selection of a more powerful actuator or other devices with an adjustable cavity becomes essential. Notably, spectral interpolation of the interference signal, such as zero-padding interpolation or chirp-Z transform, is a common method for improving data resolution. However, these methods often result in a substantial increase in computational complexity, including a higher sampling rate and a larger amount of data in Fourier analysis, which makes it difficult for them to meet the requirements of real-time measurement scenarios. We also evaluate the performance of the LFPM method using frequency-domain interpolation, and detailed results are provided in Supplementary Information 8. The measurement update rate of the current system is constrained to tens of hertz by its mechanical modulation scheme, which also limits the achievable chirp rate. However, this limitation is not intrinsic to the LFPM principle itself, which is directly applicable to other laser platforms with compatible cavity dynamics, such as laser diodes and solid-state microchip lasers. Faster tuning methods can be adopted according to their own characteristics. In future work, we will focus on the development of new light sources to achieve fast frequency-swept modulation and high update-rate measurements.

Finally, it is noteworthy that the proposed LFPM method can also provide the potential to replace the complex analysis in the frequency domain, which is typically required in conventional FMCW, with that in the time domain. The cavity dynamics of the laser feedback system induce the spontaneous generation of the harmonics of the beat signal. Importantly, these harmonics exhibit stable integer-multiple phase relationships. The detector receives the superposition of these signals. Like mode-locked signals, the detected signals exhibit sharper signal peaks in the temporal interferogram, as shown in Fig. 5c. The time intervals between these peaks directly correspond to the inverse of the beat frequency, enabling high-speed acquisition for ranging. The experimental signals are shown in Fig. 5d, targeting a mirror and an aluminum sheet. This is similar to a reported ranging system based on multi-sideband swept modulation⁶.

However, our approach achieves effective bandwidth extension instead of physically broadening the sweep range and, critically, does not require expensive external modulation devices. Additionally, in our LFPM method, it is necessary to calibrate frequency nonlinearities intrinsic to the cavity mode sweeping, such as using pre-correction techniques⁵³.

Materials and methods

Analysis of laser running frequency

According to Eqs. (1) and (2), the evolution of $E_c(t)$ and $\Phi(t)$ can be obtained by separating the real and imaginary parts⁵².

$$\frac{dE_c(t)}{dt} = \frac{B_E N(t) - \gamma_c}{2} E_c(t) + \kappa \gamma_c E_c(t - \tau) \cos[\Omega t + \Phi(t - \tau) - \Phi(t)] \quad (7)$$

$$\frac{d\Phi(t)}{dt} = \omega_c + \kappa \gamma_c \frac{E_c(t - \tau)}{E_c(t)} \sin[\Omega t + \Phi(t - \tau) - \Phi(t)] \quad (8)$$

where $d\Phi(t)/dt$ represents the optical running laser frequency $\omega(t)$. $\Phi(t - \tau)$ can be expanded in terms of time delay τ using the Taylor series. When τ is much smaller than $1/\Omega$, higher-order items except the linear term can be neglected, $\Phi(t - \tau) - \Phi(t) \approx -\omega(t)\tau$, and the electric field fluctuations can also be neglected, $E_c(t - \tau) \approx E_c(t)$. Furthermore, Eq. (8) can be simplified to Eq. (4). When the feedback strength satisfies $\kappa \gamma_c \tau < 1$, the single-mode condition, this equation yields a unique solution. The value range of the solution scales proportionally with the feedback strength and exhibits periodic oscillations. The specific analysis is described in Supplementary Information 9. To simplify the mathematical expression, the phase shift induced by frequency fluctuations can be neglected further, and the output optical field of the laser can be described by Eq. (9). Expansion using Bessel functions reveals modulation sidebands in the optical spectrum adjacent to the intrinsic mode.

$$\Delta E_c(t) \propto \cos[\omega_c t + \kappa \gamma_c / \Omega \cos(\Omega t - \omega_c \tau)] \propto \sum_{N \in \mathbb{Z}} J_N \{ \cos[(\omega_c + N\Omega)t - N\omega_c \tau] \} \quad (9)$$

Characteristics of the laser source

The laser source employed is an erbium-ytterbium co-doped distributed feedback (DFB) fiber laser, characterized by its compact architecture, prominent RO characteristics, and wide mode-hop-free tuning range. The DFB laser is pumped by a 976 nm laser diode and emits dual-port beams centered at 1545 nm. Output beams with powers of 1.2 mW and 0.3 mW are allocated for



measurement and signal analysis, respectively. An ISO is integrated into the non-probe port of the laser to suppress back-reflections from auxiliary interferometer components or photodetectors, thereby eliminating parasitic spectral signals. The free-running laser has an intrinsic linewidth of 26.4 kHz (Supplementary Information 10), as indicated by delayed self-heterodyne interferometry. Frequency-swept modulation is achieved by stretching the fiber laser cavity using a piezoelectric ceramic actuator (PZT). In the experiments, an 80 Hz symmetric triangular waveform applied to the PZT yields a sweep range of 100 GHz. A comprehensive characterization of the laser source, PZT modulation repeatability, and tuning performance is provided in Supplementary Information 11–12.

Nonlinearity calibration and distance calculation

Owing to the nonlinearity of frequency sweeping in practice, the beat frequency during a scanning ramp fluctuates with time. In this work, an unbalanced Mach–Zehnder interferometer (MZI) is used as an auxiliary interferometer to generate a resampling clock signal for nonlinearity calibration. The normalized measurement signal I_m and auxiliary signal I_a can be denoted as follows:

$$\begin{aligned} I_{m,i}(t) &= \cos[\Phi_i(t) - \Phi_i(t - \tau_m)] \\ I_{a,i}(t) &= \cos[\Phi_i(t) - \Phi_i(t - \tau_a)] \end{aligned} \quad i = \text{up, down} \quad (10)$$

where τ_m and τ_a represent the time delay originating from the distance to be measured and the difference in the optical path length of the MZI, L_{aux} . The subscript i represents the parameters in upward or downward scanning. The phase component can be expanded using a Taylor series, where higher-order terms can be neglected when

$$|\tau_a^2 \alpha| \ll 1 \quad (11)$$

where $\alpha = dv/dt$ is the chirp rate. The auxiliary signal is employed to generate a sampling clock t_k with a phase interval of π , which is expressed as follows:

$$2\pi \alpha t_k \tau_a = k\pi, k \in \mathbb{Z} \quad (12)$$

The measurement signal is sampled, yielding

$$I_{m,i}(k) = \cos\left(2\pi \frac{\tau_m}{2\tau_a} k\right) \quad (13)$$

The resampled signal in the k -domain is analyzed through the fast Fourier transform (FFT), and the distance

to be measured is revised as follows:

$$L_{N,i} = \frac{m_{N,i}}{nM_i N} L_{\text{aux}} \quad (14)$$

where M represents the length of the data after resampling for the FFT, n denotes the refractive index of the medium in the measurement path delay, and m_N indicates the peak position of the N th harmonic in the spectrum. We use the average distance from the upward and downward scans as the ranging result to compensate for the Doppler effect of ambient disturbances. Notably, in the LFPM ranging system, cavity dynamics induce extra nonlinear frequency fluctuations according to Eq. (4). However, the resampling method remains effective for the applications in this paper. The detailed derivation is provided in the Supplementary Information 13–14.

Additionally, the theoretical upper limit of the measurement range is determined by the optical path difference L_{aux} . In accordance with the Nyquist sampling criterion, the maximum measurement range for the fundamental beat signal is represented as $L_{\text{aux}}/2$. For the N th harmonic, the required sampling frequency increases by a factor of N . Consequently, the corresponding maximum measurement range is reduced to $L_{\text{aux}}/2N$.

Acknowledgements

This work is supported by the National Key R&D Program of China under Grant (No. 2024YFC2206801), China Postdoctoral Science Foundation under Grant (No. 2024M761641), and National Natural Science Foundation of China (No. 52505606).

Author details

¹State Key Laboratory of Precision Measurement Technology and Instruments, Department of Precision Instruments, Tsinghua University, Beijing, China. ²National Key Laboratory of Metrology and Calibration, Beijing Changcheng Institute of Metrology & Measurement, Beijing, China. ³Beijing Institute of Space Mechanics and Electricity, Beijing, China

Author contributions

Y.-F.W., J.L., and Y.T. conceived the idea. C.L. and Y.-F.W. performed the theoretical calculations and simulations. Y.-F.W., J.L., X.X., Y.W., X.Y., and B.X. implemented the experiments. J.H., T.W., and X.L. designed the test experiments and set up the LiDAR system. H.S. helped with the theoretical analysis. Y.T., L.C., and H.S. supervised the work. Y.-F.W. wrote the manuscript, and all the authors reviewed it.

Data availability

The data that support the findings of this study are available from the corresponding authors upon reasonable request.

Conflict of interest

Hongbo Sun is an Editor for the journal, and no other author has reported any competing interests.

Supplementary information The online version contains supplementary material available at <https://doi.org/10.1038/s41377-025-02160-x>.



Received: 1 September 2025 Revised: 2 December 2025 Accepted: 3 December 2025
Published online: 12 January 2026

References

- Na, Y. J. et al. Massively parallel electro-optic sampling of space-encoded optical pulses for ultrafast multi-dimensional imaging. *Light Sci. Appl.* **12**, 44 (2023).
- Zhang, X. S. et al. A large-scale microelectromechanical-systems-based silicon photonics LiDAR. *Nature* **603**, 253–258 (2022).
- Rogers, C. et al. A universal 3D imaging sensor on a silicon photonics platform. *Nature* **590**, 256–261 (2021).
- Ke, J. C. et al. Frequency-modulated continuous waves controlled by space-time-coding metasurface with nonlinearly periodic phases. *Light Sci. Appl.* **11**, 273 (2022).
- Li, W. H. et al. Controlling the wavefront aberration of a large-aperture and high-precision holographic diffraction grating. *Light Sci. Appl.* **14**, 112 (2025).
- Qi, Y. F. et al. 1.79-GHz acquisition rate absolute distance measurement with lithium niobate electro-optic comb. *Nat. Commun.* **16**, 2889 (2025).
- Sun, X. Y. et al. Frequency-modulated continuous-wave laser ranging beyond the limits of bandwidth and phase noise. *APL Photonics* **10**, 056118 (2025).
- Meng, W. L. et al. Resonant cavity enhanced laser frequency-swept carrier ranging method for noncooperative targets. *Photonics Res.* **13**, 1767–1775 (2025).
- Zhou, W. Y. et al. A random angle error interference eliminating method for grating interferometry measurement based on symmetry littrow structure. *Laser Photonics Rev.* **19**, 2401659 (2025).
- Wang, S. X. et al. High-performance integrated laser based on thin-film lithium niobate photonics for coherent ranging. *Laser Photonics Rev.* **18**, 2400224 (2024).
- Riemensberger, J. et al. Massively parallel coherent laser ranging using a soliton microcomb. *Nature* **581**, 164–170 (2020).
- Snigirev, V. et al. Ultrafast tunable lasers using lithium niobate integrated photonics. *Nature* **615**, 411–417 (2023).
- Zhi, Y. N. et al. Symmetrical dual-sideband oppositely chirped differential FMCW LiDAR. *Opt. Express* **31**, 38114–38131 (2023).
- Chen, H. J. et al. Highly coherent, flat, and broadband time-stretched swept source based on extra-cavity spectral shaping assisted by a booster semiconductor optical amplifier. *Opt. Express* **30**, 33708–33720 (2022).
- Liu, J. C. et al. Dynamic measurement with high precision using frequency agile spatial encoding integrated FMCW LiDAR. *ACS Photonics* **11**, 4036–4047 (2024).
- Wang, Z. et al. Cubic meter volume optical coherence tomography. *Optica* **3**, 1496–1503 (2016).
- Baumann, E. et al. Comb-calibrated laser ranging for three-dimensional surface profiling with micrometer-level precision at a distance. *Opt. Express* **22**, 24914–24928 (2014).
- Adler, D. C. et al. Three-dimensional endomicroscopy using optical coherence tomography. *Nat. Photonics* **1**, 709–716 (2007).
- Huang, D. M. et al. Fourier domain mode locked laser and its applications. *Sensors* **22**, 3145 (2022).
- Cai, Z. Y. et al. A microcomb-empowered Fourier domain mode-locked LiDAR. *Sci. Adv.* **11**, eads9590 (2025).
- Hashimoto, K. et al. Upconversion time-stretch infrared spectroscopy. *Light Sci. Appl.* **12**, 48 (2023).
- Pu, G. Q. et al. Intelligent control of mode-locked femtosecond pulses by time-stretch-assisted real-time spectral analysis. *Light Sci. Appl.* **9**, 13 (2020).
- Vasilyev, A. et al. Multiple source frequency-modulated continuous-wave optical reflectometry: theory and experiment. *Appl. Opt.* **49**, 1932–1937 (2010).
- DiLazaro, T. & Nehmetallah, G. Large-volume, low-cost, high-precision FMCW tomography using stitched DFBs. *Opt. Express* **26**, 2891–2904 (2018).
- Wang, G. C. et al. Absolute positioning by multi-wavelength interferometry referenced to the frequency comb of a femtosecond laser. *Opt. Express* **23**, 9121–9129 (2015).
- Abbasian, V. et al. Microsphere-assisted quantitative phase microscopy: a review. *Light Adv. Manuf.* **5**, 16 (2024).
- Zhu, Z. B. & Wu, G. H. Dual-comb ranging. *Engineering* **4**, 772–778 (2018).
- Nürnberg, J. et al. Dual-comb ranging with frequency combs from single cavity free-running laser oscillators. *Opt. Express* **29**, 24910–24918 (2021).
- Zhai, Y. M. et al. Dual-comb parallel sampling absolute distance measurements with an extended non-ambiguity range. *Meas. Sci. Technol.* **35**, 115023 (2024).
- Long, J. B. et al. A chip-based optoelectronic-oscillator frequency comb. *Elight* **5**, 14 (2025).
- Wang, Z. H., Yang, C. X. & Bao, C. Y. Towards fast spectroscopy using a practical all-fibre GHz dual-comb laser. *Light Adv. Manuf.* **6**, 2 (2025).
- Yang, Q. F. et al. Efficient microresonator frequency combs. *Elight* **4**, 18 (2024).
- Yao, B. C. et al. Interdisciplinary advances in microcombs: bridging physics and information technology. *Elight* **4**, 19 (2024).
- Wu, G. Z. et al. Bandwidth-enhanced LFM signal generation by period-one dynamics in a directly modulated semiconductor laser. *Opt. Lett.* **50**, 3572–3575 (2025).
- Zhang, F. M. et al. Vibration compensation of the frequency-scanning-interferometry-based absolute ranging system. *Appl. Sci.* **9**, 147 (2019).
- Lu, C., Yu, Z. H. & Liu, G. D. A high-precision range extraction method using an FM nonlinear kernel function for DFB-array-based FMCW lidar. *Opt. Commun.* **504**, 127469 (2022).
- Lin, C. X., Tan, Y. D. & Wang, Q. X. Machine learning-based prediction approach for ranging resolution enhancement of FMCW LiDAR system with LSTM networks. *Opt. Laser Technol.* **179**, 111299 (2024).
- de Chatellus, H. G. et al. Heterodyne beatings between frequency-shifted feedback lasers. *Opt. Lett.* **37**, 791–793 (2012).
- Tian, M. W. & Tan, Y. D. Intracavity-dynamics-based optical phase amplifier with over tenfold amplification. *Photonics Res.* **11**, 1892–1901 (2023).
- Li, J. et al. Toward exploring noncontinuous-state dynamics based on pulse-modulated frequency-shifted laser feedback interferometry. *Photonics Res.* **13**, 671–686 (2025).
- Otsuka, K. Self-mixing thin-slice solid-state laser Doppler velocimetry with much less than one feedback photon per Doppler cycle. *Opt. Lett.* **40**, 4603–4606 (2015).
- Wang, Y. F. et al. Laser feedback frequency-modulated continuous-wave LiDAR and 3-D imaging. *IEEE Trans. Instrum. Meas.* **72**, 7002309 (2023).
- Wang, Y. F. et al. Frequency-swept feedback interferometry for noncooperative-target ranging with a stand-off distance of several hundred meters. *Photonix* **3**, 21 (2022).
- Mason, D. et al. Continuous force and displacement measurement below the standard quantum limit. *Nat. Phys.* **15**, 745–749 (2019).
- Schreiber, K. U. et al. Variations in the Earth's rotation rate measured with a ring laser interferometer. *Nat. Photonics* **17**, 1054–1058 (2023).
- Wanner, G. Space-based gravitational wave detection and how LISA Pathfinder successfully paved the way. *Nat. Phys.* **15**, 200–202 (2019).
- Li, W. Z. et al. Harmonics-assisted optical phase amplifier. *Light Sci. Appl.* **11**, 312 (2022).
- Thomas, P. et al. Efficient generation of entangled multiphoton graph states from a single atom. *Nature* **608**, 677–681 (2022).
- Girardeau, V. et al. Nonlinear laser dynamics induced by frequency shifted optical feedback: application to vibration measurements. *Appl. Opt.* **55**, 9638–9647 (2016).
- Lacot, E. & Hugon, O. Phase-sensitive laser detection by frequency-shifted optical feedback. *Phys. Rev. A* **70**, 053824 (2004).
- Moore, E. D. & McLeod, R. R. Correction of sampling errors due to laser tuning rate fluctuations in swept-wavelength interferometry. *Opt. Express* **16**, 13139–13149 (2008).
- Taimre, T. et al. Laser feedback interferometry: a tutorial on the self-mixing effect for coherent sensing. *Adv. Opt. Photonics* **7**, 570–631 (2015).
- Zhang, X. S., Pouls, J. & Wu, M. C. Laser frequency sweep linearization by iterative learning pre-distortion for FMCW LiDAR. *Opt. Express* **27**, 9965–9974 (2019).

